Biosensors and Bioelectronics 62 (2014) 127–133

Contents lists available at ScienceDirect

Biosensors and Bioelectronics

journal homepage: www.elsevier.com/locate/bios

Synthesis of zinc oxide nanoparticles on graphene–carbon nanotube hybrid for glucose biosensor applications

Kuo-Yuan Hwa [a,b,c,*], Boopathi Subramani [a]

[a] Department of Molecular Science and Engineering, National Taipei University of Technology, Taipei, Taiwan
[b] Institute of Organic and Polymeric Materials, National Taipei University of Technology, Taipei, Taiwan
[c] Centre for Biomedical Industry, National Taipei University of Technology, Taipei, Taiwan

ARTICLE INFO

Article history:
Received 14 May 2014
Received in revised form
11 June 2014
Accepted 12 June 2014
Available online 17 June 2014

Keywords:
Biosensor
Carbon nanotube
Glucose oxidase
Graphene
Zinc oxide

ABSTRACT

Synthesis of zinc oxide nanoparticles incorporated graphene–carbon nanotubes hybrid (GR–CNT–ZnO) through a simple, one-pot method is demonstrated. The as-synthesized GR–CNT–ZnO composite is applied to fabricate an enzyme based glucose biosensor. The GOx immobilized on GR–CNT–ZnO composite exhibits well-defined redox peaks with a peak potential separation (ΔE_p) of about 26 mV with enhanced peak currents, indicating a fast electron transfer at the modified electrode surface. The cyclic voltammetry measurements revealed that the modified film has high electrocatalytic ability towards glucose detection in the presence of oxygen. The proposed sensor has a wide linear detection range from 10 μM to 6.5 mM of glucose with a limit of detection (LOD) of 4.5 ($\pm$0.08) μM. In addition, the sensor possessed appreciable repeatability, reproducibility and remarkable stability for the sensitive determination of glucose. The practicality of this sensor has been demonstrated in human serum samples, with results being in good agreement with those determined using a standard photometric method.

1. Introduction

The applications of biocompatible nanomaterials for enzymatic glucose sensors were explored as they help the enzymes to retain its activity and to augment direct electron transfer between the active site of the enzyme and the electrode (Umar, 2010). Carbon nanotubes (CNTs) and graphene (GR) are the most widely used nanomaterials in electrochemical sensors due to their conductivity, chemical stability, flexibility and low cost. GR is a two dimensional layer of graphite with sp^2 carbon atoms arranged in a hexagonal lattice. It has attracted tremendous research interest among theoretical and experimental scientists due to its unique electrical properties and rich surface chemistry (Geim and Novoselov, 2007). The distinct properties of GR have led to its application in developing devices such as field-effect transistors (Li et al., 2008a, b), photovoltaic devices (Williams and Kamat, 2009), capacitors (Stoller et al., 2008) and electrochemical sensors (Zhou et al., 2009). The GR sheets have low polarity, hydrophobic surfaces with high π-electron density. These properties make GR to be useful for immobilizing molecules through covalent (Si and Samulski, 2008) and non-covalent interactions (Stankovich et al., 2006). GR can be produced through chemical or thermal reduction of graphene oxide (GO) (Shao et al., 2010). The chemical reduction paves the way for deposition of GR from solution, enabling devices to be fabricated on any surface (Eda et al., 2008). The hydrophilic properties of GO make it an exceptional material to suspend the CNTs in aqueous medium. The hybridization of GO and CNTs is expected to have synergistic effects as they have similar structural and physical properties (Sharma et al., 2012). On the other hand, CNTs are the rolled version of GR which are single walled (SWCNTs) and multiwalled carbon nanotubes (MWCNTs). CNTs are widely used in electrochemical sensors and biosensors applications due to their distinct electrochemical properties such as high electrocatalytic activity and high electron-transfer rate (Lin et al., 2004). Thus, CNTs and GR have a great potential as supporting materials for enzymes. Along with carbon supports, metal oxide nanostructures can be used to adsorb enzymes due to their high specific surface area, biocompatability and chemical stability. The nanostructured metal oxides coupled with different redox enzymes were used for fabricating biosensors (Wan et al., 2004). Among different metal oxides, ZnO nanostructures have been used in glucose sensors as they have advantages such as non-toxic, electrochemical activity and high electron transfer rate (Zang et al., 2007).

* Corresponding author at: Department of Molecular Science and Engineering, National Taipei University of Technology, Taipei, Taiwan. Tel.: +886 2 27712171; fax: +886 2 27317174.
E-mail address: kyhwa@ntut.edu.tw (K.-Y. Hwa).

http://dx.doi.org/10.1016/j.bios.2014.06.023
0956-5663/

The electrochemical glucose sensors are most widely used for measuring blood glucose levels in diabetic patients because of their high sensitivity, selectivity, rapidness, fidelity, portability and low cost (Oliver et al., 2009). The major challenge in the fabrication of electrochemical glucose sensors is the immobilization of model enzyme, glucose oxidase (GOx) on the electrode surface through effective electrical communication between GOx and the transducer without compromising the mechanical stability and catalytic activity of the enzyme (Chen et al., 2013). To attain these key features, various materials and methods have been used for the surface modification of electrodes (Liu et al., 2013; Periasamy et al., 2011). Glucose oxidase (GOx) is highly selective for glucose in biological samples.

In this study, we utilized CNTs, GR and ZnO to immobilize GOx for the development of a voltammetric gluose sensor. GO–CNT composite was prepared by a simple solution based approach, then the GR–CNT–ZnO composite was obtained by the simultaneous reduction of GO and zinc acetate using sodium borodihydride ($NaBH_4$). GOx was successfully immobilized on the GR–CNT–ZnO composite and it was employed for the fabrication of a voltammetric glucose sensor. The practicality of the proposed GR–CNT–ZnO/GOx sensor was successfully demonstrated in human serum sample.

2. Experimental

2.1. Preparation of GR–CNT–ZnO composite

The preparation of GR–CNT–ZnO composite is shown in Scheme 1. Briefly, graphite oxide was prepared by modified Hummer's method (Hummers and Offeman, 1958) and subsequently exfoliated to GO via ultrasonication for 2 h. Then, GO was centrifuged at 3000 rpm for 30 min and homogenous dispersion of GO was collected. About 10 mg of CNTs was added to 5 mL GO (1 mg mL^{-1}) and ultrasonicated for 2 h. The yellowish brown color of GO changed to black color, indicating the formation of GO–CNT composite. GO–CNT was mixed with zinc acetate (5 mM) and stirred for 3 h. Then NaOH solution was added to adjust the pH to 10. The resulting mixture was stirred for 30 min. Afterwards, 35 mg of $NaBH_4$ was added and vigorously stirred for 30 min and then heated at 130 °C for 6 h. After completion of the reduction process, the final product was filtered and washed with copious amount of water to get pure GR–CNT–ZnO composite and finally dried overnight. The obtained GR–CNT–ZnO composite was dispersed in ethanol (0.5 mg mL^{-1}) and used for further experiments. As a control, GR–CNT composite was prepared by following the same procedure but without adding zinc acetate.

2.2. Fabrication of GR–CNT–ZnO composite modified GCE

The GCE surface was polished with alumina slurry (0.05 μm) using a Buehler polishing kit and ultrasonicated in water for 5 min and dried. 5 μL of GR–CNT–ZnO composite was drop casted on the surface of pre-cleaned GCE and dried at ambient conditions. Then 6 μL of GOx (10 mg mL^{-1} in PBS (pH 7)) was drop casted onto the GR–CNT–ZnO composite modified GCE and dried at room temperature for 1 h. Finally, the GR–CNT–ZnO/GOx modified GCE was washed with distilled water to remove loosely adsorbed GOx. As a control, GOx immobilized on GR, CNT, ZnO, GR–ZnO, CNT–ZnO and GR–CNT electrodes was also prepared.

3. Results and discussion

3.1. Surface morphological study of GR–CNT–ZnO composite

Fig. S1 shows the SEM images of GO (A) and GO–CNT hybrid (B). The SEM image of GO clearly indicates characteristic wrinkled sheet like morphology. SEM image of the GO–CNT hybrid portrays the CNTs networks decorated with GO sheets. The strong π–π non-covalent interaction between hydrophobic surface of GO and tubular structure of CNTs is the critical driving force towards the formation of a stable GO–CNT hybrid (Mani et al., 2013). The SEM image of the GR–CNT–ZnO composite (Fig. 1A) shows that GR–CNT sheets are decorated with numerous ZnO nanoparticles. A higher magnification image (Fig. 1B) clearly reveals the formation of ZnO nanoparticles on the GR–CNT surface. The uniform shape and size of ZnO (~50–80 nm) show the controlled synthesis of ZnO nanoparticles.

Moreover, the TEM image (Fig. S2) of GO–CNT shows that CNTs are wrapped by thin GO sheets, indicating the formation of stable

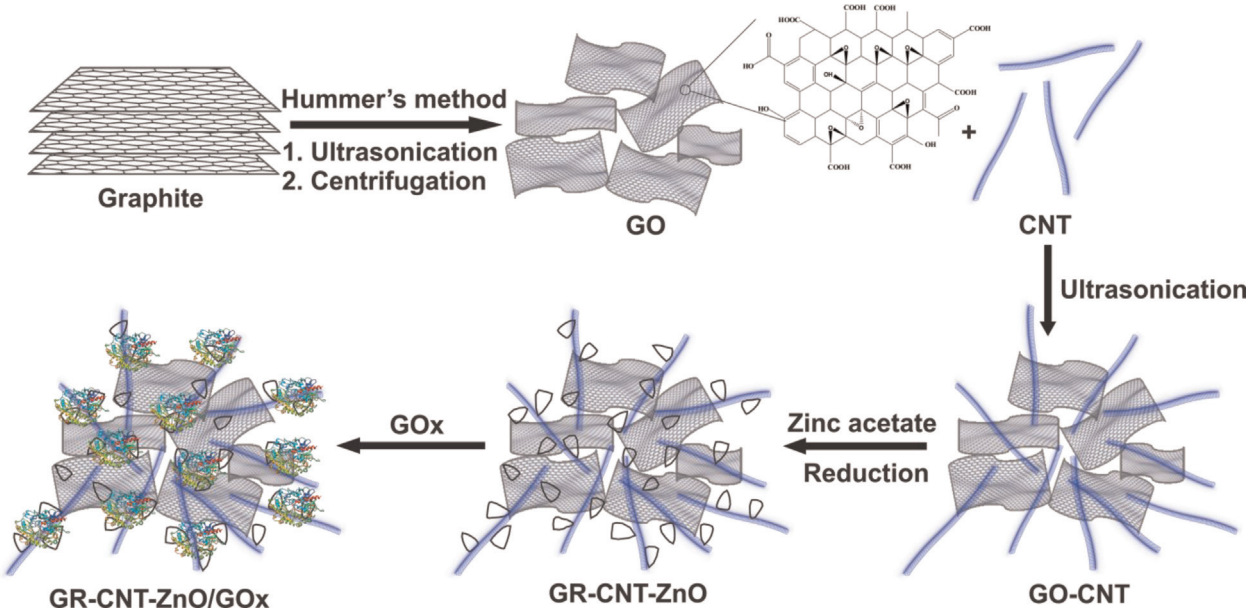

Scheme 1. Schematic representation of the preparation of GR–CNT–ZnO composite.

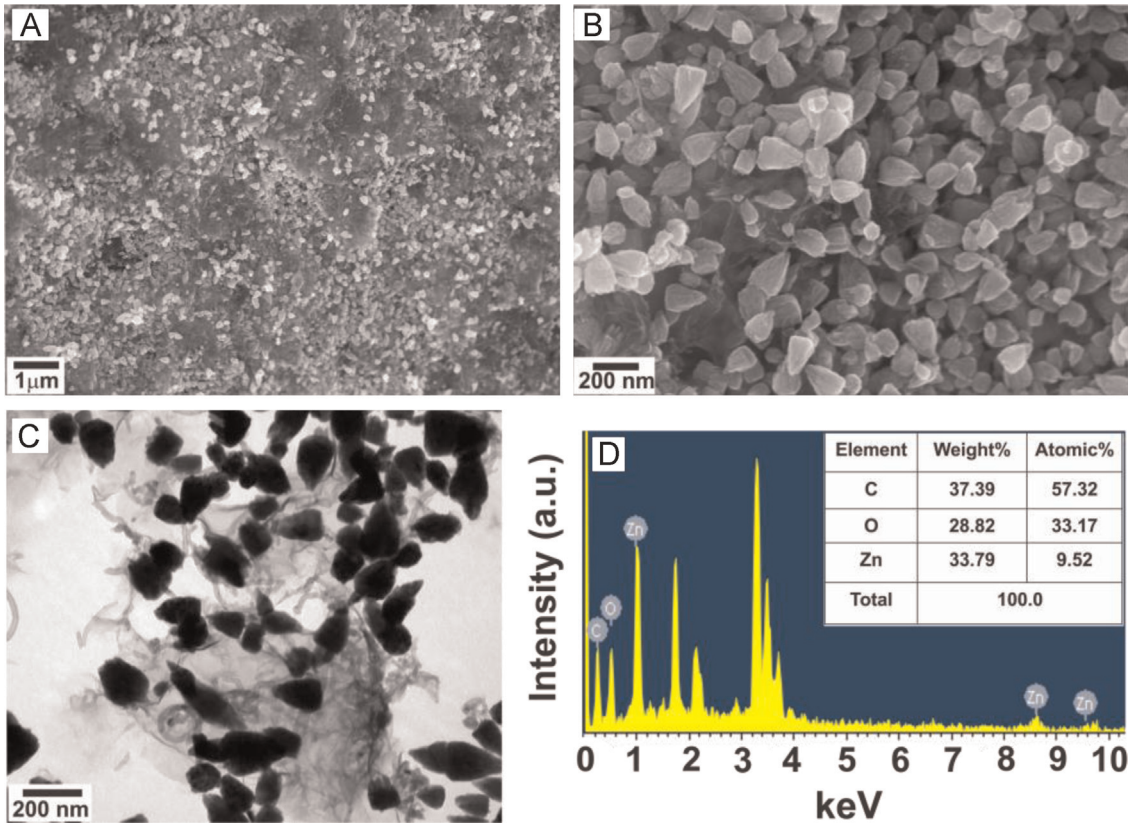

Fig. 1. SEM (A, B), TEM (C) and EDX (D) images of GR–CNT–ZnO composite.

composite. The TEM image of GR–CNT–ZnO composite (Fig. 1C) illustrates the incorporation of ZnO nanoparticles within GR–CNT networks. Based on the SEM and TEM results, it is apparent that GR–CNT is a good supporting material to anchor ZnO nanoparticles.

3.2. Elemental analysis and spectroscopic characterization of GR–CNT–ZnO/GOx composite

EDX spectroscopic measurements were used to analyze the elemental composition of the composite. The EDX spectra of GO and GO–CNT hybrid films are given in Fig. S3. GO contains 59.16% of C and 40.84% of O, while GO–CNT hybrid contains 80.76% C and 19.24% O. The increase in carbon percentage from 59.16% to 80.76% is due to the incorporation of CNTs with GO. GR–CNT–ZnO composite (Fig. 1D) contains 37.39%, 28.82% and 33.79% of C, O and Zn, respectively. These results confirm the formation of ZnO with GR–CNT hybrid material. The decrease in C content from 80.76% to 37.39% might affect the hydrophobic interaction of the network.

The XRD pattern of GO exhibits a sharp diffraction peak at 2θ of 11.3°, which is attributed to the large interlayer d-spacing ~8.12 Å (curve a, Fig. 2A). GO–CNT hybrid exhibits a diffraction peak at 2θ of around 26.1° (curve b, Fig. 2A), which is ascribed to the graphitic network. The XRD pattern of GR–CNT–ZnO composite (curve c, Fig. 2A) is assigned to the characteristic hexagonal wurtzite structure of ZnO (JCPDS, 36-1451), indicating the formation of ZnO on the GR–CNT hybrid network (Raoufi, 2013).

The ATR-FTIR spectrum of GO (curve a, Fig. 2B) shows the presence of typical vibrational modes of oxygen functional groups. The oxygen functionalities such as hydroxyl, carbonyl, epoxy and alkene groups showed their stretching vibrations at 3360, 1725, 1233 and 1620 cm^{-1} respectively. ATR-FTIR spectrum of GO–CNT hybrid (curve b, Fig. 2B) exhibits similar characteristic peaks, revealing the incorporation of GO along with CNTs. The intensity of all these characteristic peaks significantly decreased in the spectrum of GR–CNT–ZnO (curve c, Fig. 2B), indicating the removal of oxygen functionalities upon chemical reduction.

3.3. Direct electrochemistry of GOx on GR–CNT–ZnO composite

Fig. 3A displays the cyclic voltammograms (CVs) acquired at GR/GOx (a), CNT/GOx (b), ZnO/GOx (c) and GR–CNT–ZnO/GOx (d) films modified GCEs in PBS (pH 7) at a scan rate of 50 mV s^{-1}. Electrochemical parameters of the GOx redox peaks such as peak currents (anodic peak current (I_{pa}) and cathodic peak current (I_{pc})), formal potential ($E^{\circ\prime}$) and peak potential separation value (ΔE_p) are given in Table S1. The redox peaks of GOx refer to the direct electron transfer between flavin adenine dinucleotide (FAD) and its reduced form, $FADH_2$ at the modified electrodes. The direct electron transfer ability of GOx at these modified electrodes is in the order of GR–CNT–ZnO/GOx > CNT/GOx > GR/GOx > ZnO/GOx. GR–CNT–ZnO/GOx exhibited enhanced redox peaks with highest I_{pc} and I_{pa} and lowest ΔE_p values than the other modified electrodes. The outstanding direct electron transfer ability of GOx at the GR–CNT–ZnO modified electrode surface is attributed to the large surface area, favorable orientation of GOx, good biocompatibility, and high electrical conductivity of GR–CNT–ZnO.

We noted that the isoelectric point (IEP) of ZnO is 9.5 (Umar, 2010) whereas that of GOx is 4.2. At pH 7, ZnO surface is positively charged, while GOx surface is negatively charged. Therefore, electrostatic interactions between positively charged ZnO nanostructures with negatively charged surface of GOx lead to efficient immobilization of GOx. Moreover, GR–CNT acts as good support for the growth of ZnO nanostructures through the anchoring of Zn^{2+} ions with the functional groups of GO followed by the in situ reduction by $NaBH_4$. However, GOx did not show direct electrochemistry at ZnO/GOx due to the poor stability of ZnO film. We

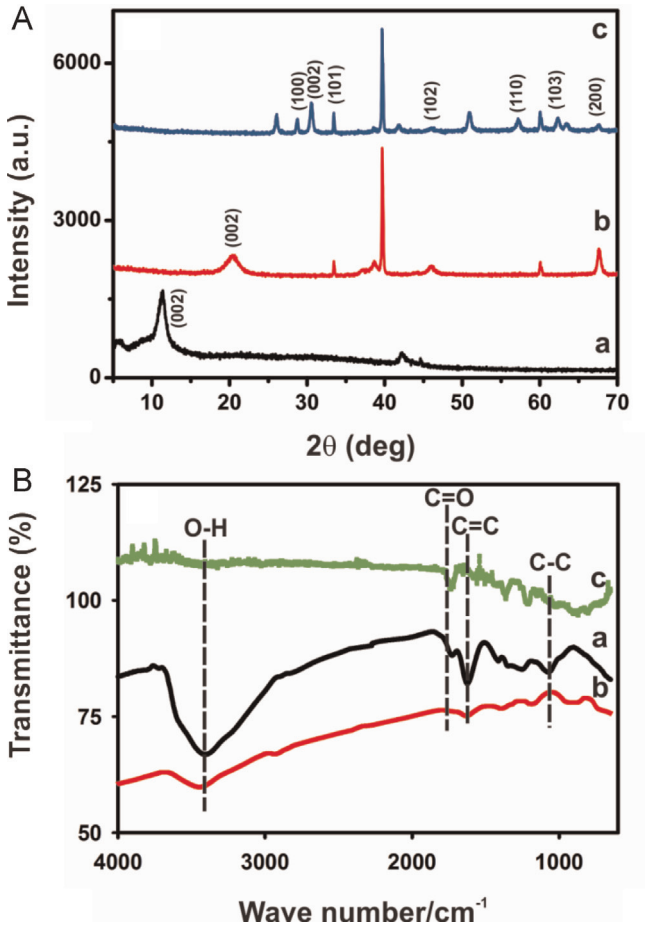

Fig. 2. XRD (A) and ATR-FTIR (B) images of GO (a), GR–CNT (b) and GR–CNT–ZnO composite.

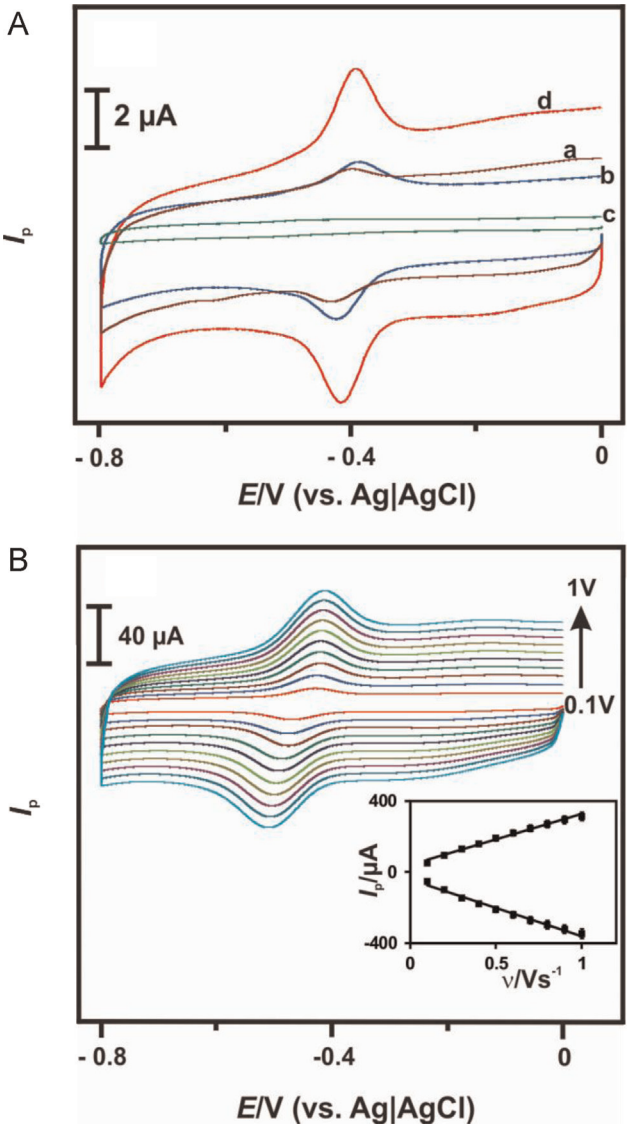

Fig. 3. (A) CVs obtained at GR/GOx (a), CNT/GOx (b), ZnO/GOx (c) and GR–CNT–ZnO/GOx (d) film modified GCEs in PBS of pH 7 at the scan rate of 50 mV s^{-1}. (B) CVs of GR–CNT–ZnO/GOx film modified GCEs in PBS (pH 7) at various scan rates from inner to outer are 0.1 to 1 V s^{-1}. Inset: plot of I_{pa} and I_{pc} versus scan rates.

also evaluated the key roles played by the nanomaterials and their possible combinations as support in enhancing the direct electrochemistry of GOx. Fig. S4 shows the CVs obtained at GR–ZnO/GOx (a), CNT–ZnO/GOx (b) and GR–CNT/GOx (c) films modified GCEs in PBS (pH 7). The electrochemical parameters such as I_{pa}, I_{pc}, $E^{\circ\prime}$ and ΔE_p obtained for GOx at these electrodes are provided in Table S1. The direct electron transfer ability of GOx at these electrodes is in the order of GR–CNT/GOx > CNT–ZnO/GOx > GR–ZnO/GOx.

The enhanced direct electron transfer of GOx at the GR–CNT support is due to the excellent electrical conductivity of GR and CNTs. Therefore, we chose GR–CNT as the supporting material for ZnO to prepare GR–CNT–ZnO composite for immobilizing GOx. The as-immobilized GOx exhibited promising direct electrochemistry (Table S1). Moreover, the stability of the GR–CNT–ZnO/GOx/GCE was studied by recording 200 successive cyclic voltammograms in PBS (pH 7) at a scan rate of 50 mV s^{-1}. 94.1% of the initial peak currents were maintained even after 200 successive potential cycles, which confirmed the stability of GOx at the GR–CNT–ZnO composite. Perhaps, two kinds of interactions are possible between GOx and composite film: (1) simple physical adsorption between GOx and the nanostructured composite film (Tang et al., 2004), and (2) electrostatic interactions between positively charged ZnO nanostructures with negatively charged GOx at pH 7 (Umar, 2010). It has been reported that the zeta potential (ζ) values of the pristine CNTs and GR are −29, and −36 mV, respectively at pH 7 (Jiang and Gao, 2003; Li et al., 2008a, b). So, the GR–CNT composite will have negative surface charges. The zeta potential of ZnO at pH 7 is +18 mV (Mohd Omar et al., 2014), revealing the surface with positive charges. Thus, the positively charged ZnO is attached with the negatively charged GR–CNT composite through the electrostatic interactions. The GOx has negative surface charges since their zeta potential value is −32.91 mV (Xiaofei et al., 2014). Hence, the negatively charged GOx was immobilized on the positively charged ZnO particles through electrostatic interactions.

The electrochemical active surface areas of the ZnO–GR–CNT, ZnO–GR and ZnO–CNT electrodes were estimated using Randles–Sevcik equation employing $K_3[Fe(CN)_6]$ as a model redox mediator (Table S2) (Liu et al., 2014). The active surface area of the ZnO–GR–CNT (0.186 cm^2) is higher than that of GR–ZnO (0.121 cm^2), CNT–ZnO (0.156 cm^2), and GR–CNT (0.171 cm^2) electrodes, which allows for high GOx loading.

Fig. 3B shows the CVs of GR–CNT–ZnO composite film modified GCE in PBS (pH 7) at various scan rates from 0.1 to 1 V s^{-1}. The redox peak currents increased linearly with scan rate. The plot of peak current versus scan rates showed good linear relationship, revealing that the electron transfer process of GOx is a surface confined process (inset to Fig. 3B). The linear regression equations can be expressed as I_{pa} (μA) = 288.96 ν (μA/V) + 39.5; R^2 = 0.990 for

anodic current, and I_{pc} (μA) = −320.42ν (μA/V) − 40.62; R^2 = 0.989, for cathodic current, where ν is the scan rate.

We calculated the amount of electroactive GOx (Γ) present on the GR–CNT–ZnO modified electrode surface from the slope of peak currents versus scan rate by the following equation (Bard and Faulkner, 2001):

$$I_p = n^2F^2\nu A\Gamma/4RT \quad (1)$$

where ν (V s^{-1}) is the scan rate and A (cm^2) is the electrode surface area. The constants R, T and F have their usual meanings (R = 8.314 J K^{-1} mol^{-1}, T = 298 K, and F = 96485 C mol^{-1}). Assuming the number of electrons transferred (FAD/FADH$_2$ redox reaction) as 2, the amount of electroactive GOx (Γ) has been calculated to be 1.21×10^{-9} mol cm^{-2}. The Γ value calculated at the GR–CNT–ZnO/GOx is significantly higher than the other films modified electrodes (Mani et al., 2013; Unnikrishnan et al., 2013; Kang et al., 2009) (Table S3). In addition, the apparent heterogeneous electron transfer rate constant (k_s) of GOx at the composite film modified GCE was calculated using Laviron equation (Bard and Faulkner, 2001):

$$\text{Log } K_s = \alpha \log(1-\alpha) + (1-\alpha)\log\alpha - \log(RT/nF\nu) - \alpha(1-\alpha) \times nF\Delta E_p/2.3RT \quad (2)$$

where ν (V s^{-1}) is the scan rate, and α is the charge transfer coefficient (~0.5). The k_s value of GR–CNT–ZnO/GOx composite film modified GCE is calculated to be 5.544 s^{-1}, which is higher than the other reported modified electrodes (Mani et al., 2013, Unnikrishnan et al., 2013, Kang et al., 2009). The high k_s value obtained at the GR–CNT–ZnO modified electrode suggests faster electron transfer rate between the active sites of GOx and electrode.

3.4. Effect of solution pH on the modified electrode

We studied the performance of modified electrodes in various pHs from 1 to 11 (Fig. S5). GOx exhibits redox peaks in wide pH range (1–11); however, it exhibits stable redox peaks only at pH 7 as supported by the stability results which are discussed in Section 3.7. GOx denatured at low and high pH values, as observed with decreased redox peak currents when performing continuous potential cycles (data not shown). Besides, the plot of pH versus $E^{\circ\prime}$ (inset in Fig. S5) exhibited a linear plot with the linear regression equation expressed as $E^{\circ\prime}/V = -0.017/V - 0.053$ pH/(V/pH). Notably, the slope of the plot was −53.0 mV/pH, which is close to the theoretical value of −58.6 mV/pH involving equal number of protons and electrons. Thus, we conclude that the redox process of GOx is reversible with the involvement of two electrons and two protons (Mani et al., 2013).

3.5. Electrocatalytic determination of glucose

The electrocatalytic activity of the GR–CNT–ZnO/GOx modified GCE was studied by CV in oxygen saturated PBS (pH 7) containing various concentrations of glucose (0.5–5 mM) (Fig. S6). The GR–CNT–ZnO/GOx electrode exhibits a new cathodic peak at −0.55 V in addition to FAD to FADH$_2$ reduction peak at −0.45 V in oxygen saturated PBS (Fig. S6) whereas in nitrogen saturated PBS, GR–CNT–ZnO/GOx electrode shows only one cathodic peak at −0.45 V, which is attributed to the reduction of FAD to FADH$_2$ (Fig. 3A). As a control, we also observed a similar cathodic peak at the GR–CNT–ZnO modified electrode without GOx at −0.54 V in oxygen saturated PBS (data not shown). But, we did not observe any peak at the GR–CNT–ZnO electrode at −0.45 V in N_2 saturated solution. This clearly reveals that the cathodic peak of both the GR–CNT–ZnO (at −0.54 V) and GR–CNT–ZnO/GOx (at −0.55 V) electrodes in O_2 saturated PBS should be ascribed to the oxygen reduction reaction. To confirm the peak at −0.45 V as FAD to FADH$_2$ reduction peak, CVs were recorded in GR–CNT–ZnO/FAD modified electrode in the presence of oxygen saturated PBS. As shown in inset 'a' of Fig. S6, GR–CNT–ZnO/FAD modified electrode shows a defined reduction peak at −0.47 V in O_2 saturated PBS, which is ascribed to the FAD/FADH$_2$ redox process. Therefore the peak observed at −0.45 V in Fig. S6 must come from the FAD reduction, while the cathodic peak observed at the potential of −0.55 V could be due to the oxygen reduction reaction. These mechanistic results were also in consistent with the previous reports (Bai et al., 2014; Ghica et al., 2009).

When 0.5 mM glucose was added the cathodic peak current (−0.55 V) started to decrease and it decreased linearly with increase in glucose concentrations over the range of 0.5–6 mM. The decrease in oxygen content upon addition of glucose can be explained as follows: (Wang, 2008)

$$\text{GOx(FAD)} + \text{glucose} \rightarrow \text{GOx(FADH}_2) + \text{gluconolactone} \quad (3)$$

$$\text{GOx(FADH}_2) + O_2 \rightarrow \text{GOx(FAD)} + H_2O_2 \quad (4)$$

$$O_2 + 4H^+ + 4e^- \rightarrow 2H_2O \quad (5)$$

The activity of the immobilized GOx towards determination of glucose in terms of temperature was investigated in the temperature range 25–65 °C. Fig. S7 shows that the glucose sensing ability is predominant at 55 °C, which is also consistent with the literature reports (Arslan et al., 2012). The activity of the GOx was determined by monitoring the decrease in the cathodic peak currents (I_{pc}). We observed a maximum decrease in the I_{pc} value at 55 °C, revealing its higher activity. Even though GOx showed relatively better performance at 55 °C, stability of the enzyme at higher temperature is a major concern for long term use. In addition, considering the practical difficulties associated in operating the sensor at higher temperature in real samples and to avoid the denaturation of the enzyme, we investigated the activity of the sensor at ambient conditions (25 °C).

The electrocatalytic activities of ZnO/GOx, GR–CNT/GOx and GR–CNT–ZnO/GOx were examined in the presence of 3 mM glucose and the activity, stability, efficiency and durability were evaluated and the results are given in Table S4. The electrocatalytic activity of these electrodes exhibited the following order: GR–CNT–ZnO/GOx > GR–CNT/GOx > ZnO/GOx. The order follows similar trend that was observed in the studies of GOx direct electrochemistry discussed in Section 3.3. Consequently, in all the perspective, GR–CNT–ZnO/GOx exhibited maximum electrocatalytic performance towards determination of glucose.

The determination of glucose at the GR–CNT–ZnO/GOx/GCE was done by differential pulse voltammetry (DPV) in oxygen saturated PBS (pH 7) (Fig. 4). The most widely used technique for enzyme based sensors is amperometry (Wang, 2008). The GOx used in amperometric sensors oxidize glucose to gluconic acid and H_2O_2 in the presence of oxygen; however, maintaining a stable oxygen concentration is difficult in hydrodynamic amperometric sensors due to the uncontrolled diffusion of oxygen during the rotation of the electrode. We used DPV as it offers great sensitivity and reproducibilty and also no hydrodyanamic motion involved in this technique. A sharp cathodic peak at ~−0.44 V was observed in oxygen saturated PBS (curve a, Fig. 4), which was decreased with increase in glucose concentrations due to decrease in oxygen content in the solution as explained by Eqs. (3)–(5). A calibration plot between glucose concentrations and their respective peak currents gave a linear response (Fig. 4). The linear regression equation can be expressed as I_p (μA) = −0.3865 (±0.051)

[glucose]/ ($\mu A\ mM^{-1}$) − 0.1427 (± 0.038)/μA, R^2 = 0.983. The linear concentration range of glucose was between 10 μM and 6.5 mM. From slope of the calibration plot, the sensitivity of the sensor was calculated to be 5.362 (± 0.072) $\mu A\ mM^{-1}\ cm^{-2}$. The limit of detection (LOD) is 4.5 (± 0.08) μM. The excellent analytical parameters such as wide linear range, low detection limit and high sensitivity revealed the ability of the sensor towards determination of glucose. Table 1 lists the important analytical parameters compared with other GR and CNTs based glucose sensors. The result explains that the GR–CNT–ZnO composite modified electrode exhibits quite comparable or better performance than other modified electrodes.

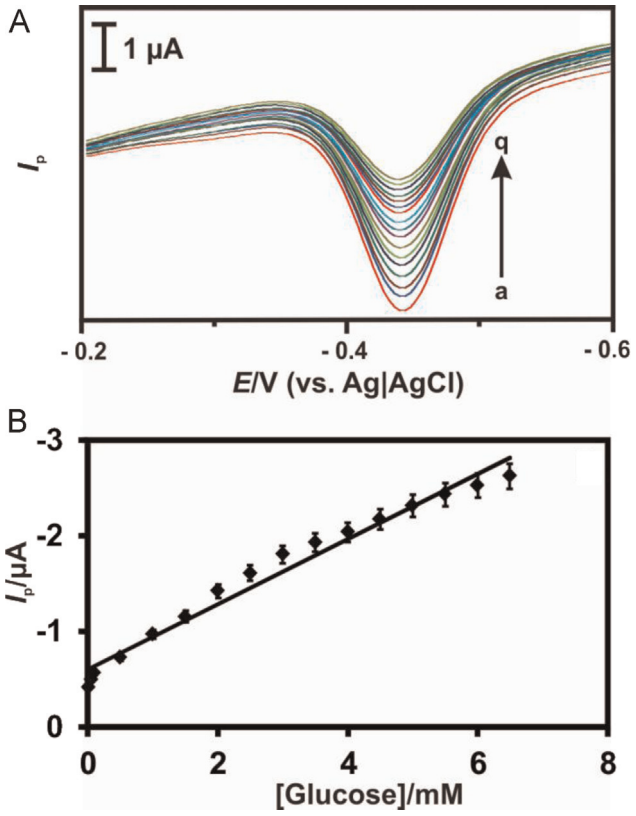

Fig. 4. (A) DPV of GR–CNT–ZnO/GOx film modified GCEs in the absence (a) and presence of glucose (b to q are 10 μM to 6.5 mM). (B) Calibration plot of [glucose] versus peak current.

3.6. Real sample analysis

To investigate the practicality of the sensor, we used the proposed sensor to determine the amount of glucose present in human blood serum sample. The glucose concentration in the serum was pre-determined as 4.46 mM using a standard commercial photometric analyzer (ROCHE COBAS C 111 ANALYZER). The DPV analysis of serum sample was performed using GR–CNT–ZnO/GOx modified GCE. Aliquots of glucose solution were added to five-fold diluted human serum and the cathodic peak currents were recorded. The glucose concentration in the serum sample has been determined to be 4.7 mM, which is in close agreement with the value determined by the standard method. Thus, the proposed sensor has excellent practical feasibility towards determination of glucose in the blood serum sample.

3.7. Stability, repeatability and reproducibility studies

We studied the storage stability of the sensor by monitoring redox peak currents everyday by storing the sensor in refrigrator at 4 °C. 94.6% peak current was retained even after 4 weeks, revealing the good storage stability of the sensor. The strong interaction of GOx with the composite film retained the biocompatiblity of GOx for longer time. Repeatability and reproducibility of the sensor were carried out by recording DPV in PBS (pH 7) with 3 mM glucose. The sensor exhibited a relative standard deviation (RSD) of 2.75% for five repetitive measurements, suggesting a good repeatability of the sensor. In addition, the sensor exhibited appreciable reproducibility with an RSD of 3.24% for five different modified electrodes.

4. Conclusion

We prepared the GR–CNT–ZnO composite by an one-pot chemical reduction route. The GR–CNT–ZnO composite was characterized by SEM, EDX, TEM, XRD, AT-FTIR and electrochemical techniques. GOx was immobilized on the composite without using any binders and cross-linking agents. Direct electrochemistry of GOx was observed on the prepared composite with fast electron transfer (k_s = 5.544 s^{-1}). The GOx immobilized modified electrode showed good electrocatalytic activity towards determination of glucose in the presence of oxygen. The good electron transfer efficiency and electrocatalytic activity of the electrode may extend its application to biofuel cells. Moreover, the proposed sensor exhibited excellent analytical parameters. The LOD of this sensor

Table 1
Comparison of analytical parameters of GR–CNT–ZnO/GOx film modified GCE with other GOx based modified GCEs.

Electrode material	Technique	Sensitivity	Linear range (mM)	LOD[a] (μM)	Ref.
GR–CNT–ZnO–GOx	DPV	5.36 (± 0.072) $\mu A\ mM^{-1}\ cm^{-2}$	0.01–6.5	4.5 (± 0.08)	This work
RGO[b]–GOx	Amperometry	1.85 $\mu A\ mM^{-1}\ cm^{-2}$	0.1–27	–	Kang et al. (2009)
ERGO[c]–MWCNT[d]/GOx/Nf	Amperometry	7.95 $\mu A\ mM^{-1}\ cm^{-2}$	0.01–6.5	4.7	Mani et al. (2013)
Gelatin–MWCNT–GOx	Amperometry	2.47 $\mu A\ mM^{-1}\ cm^{-2}$	6.30–20.1	–	Periasamy et al. (2011)
MWCNT–Nafion–GOx	Amperometry	10 nA mM^{-1}	0.1–0.4	24	Tsai et al. (2005)
Cellulose–MWCNT–GOx	Amperometry	6.57 $\mu A\ mM^{-1}\ cm^{-2}$	0.05–1	–	Wu et al. (2009)
MWCNTs@SnO_2–Au/GOx	Amperometry	–	4.0–24	5	Li et al. (2009)
PVF[e]–MWCNT–GOx	LSV[f]	9.5 mA M^{-1}	400–8	41	Sljukic et al. (2006)
Nafion/GOx/ZnO–Nano-graphene	FFTCCV[g]	–	0.0001–0.02	0.02	Norouzi et al. (2011)
ZnO–GOx/Si	DPV	–	0.1–10	–	Weber et al. (2008)

[a] LOD—limit of detection.
[b] RGO—reduced graphene oxide.
[c] ERGO—electrochemically reduced graphene oxide.
[d] MWCNT—multiwalled carbon nanotubes.
[e] PVF—poly(vinylferrocene).
[f] LSV—linear sweep voltammetry.
[g] FFTCCV—fast Fourier transformation continuous cyclic voltammetry.

is 4.5 μM (±0.08) and its sensitivity is 5.362 (±0.072) μA mM^{-1} cm^{-2}. In addition, the sensor possessed appreciable stability, repeatability and reproducibility with good RSD values. The proposed composite used in this study will be extended to detect glucose in bioethanol production from lignocellulose fermentation, in our future work. This nanocomposite may be used to immobilize other enzymes, proteins or DNA for various biological and electrochemical applications.

Acknowledgments

This study was supported by the grants from National Taipei University of Technology (NTUT-100-140-01) to K.-Y. Hwa. Our sincere thanks to Prof. Chang Shu-Mei for helping us to perform the FTIR spectroscopy. The authors like to thank Dr. Binesh Unnikrishnan, Dr. Arun Prakash Periasamy and Dr. Veerappan Mani for their help throughout this project. We also thank Ms. Sasipriya Kathirvel and Mr. Rajkumar Devasenathipathy for their assistance in this work.

Appendix A. Supplementary information

Supplementary data associated with this article can be found in the online version at http://dx.doi.org/10.1016/j.bios.2014.06.023.

References

Arslan, H., Ozdemir, M., Zengin, H., Zengin, G., 2012. Int. J. Electrochem. Soc. 7 (10), 10205–10214.
Bai, Y.-F., Xu, T.-B., Luong, J.H.T., Cui, H.-F., 2014. Anal. Chem. 86 (10), 4910–4918.
Bard, A.J., Faulkner, L.R., 2001. Electrochemical Methods, second ed. John Wiley & Sons, Inc., New York.
Chen, C., Xie, Q.J., Yang, D.W., Xiao, H.L., Fu, Y.C., Tan, Y.M., Yao, S.Z., 2013. RSC Adv. 3 (14), 4473–4491.
Eda, G., Fanchini, G., Chhowalla, M., 2008. Nat. Nanotechnol. 3 (5), 270–274.
Geim, A.K., Novoselov, K.S., 2007. Nat. Mater. 6 (3), 183–191.
Ghica, M.E., Pauliukaite, R., Fatibello-Filho, O., Brett, C.M.A., 2009. Sens. Actuators B 142 (1), 308–315.
Hummers, W.S., Offeman, R.E., 1958. J. Am. Chem. Soc. 80 (6), 1339.
Jiang, L., Gao, L., 2003. Carbon 41 (15), 2923–2929.
Kang, X., Wang, J., Wu, H., Aksay, I.A., Liu, J., Lin, Y., 2009. Biosens. Bioelectron. 25 (4), 901–905.
Li, D., Müller, M.B., Gilje, S., Kaner, R.B., Wallace, G.G., 2008a. Nat. Nanotechnol. 3 (2), 101–105.
Li, F.H., Song, J.X., Li, F., Wang, X.D., Zhang, Q.X., Han, D.X., Ivaska, A., Niu, L., 2009. Biosens. Bioelectron. 25 (4), 883–888.
Li, X., Wang, X., Zhang, L., Lee, S., Dai, H., 2008b. Science 319 (5867), 1229–1232.
Lin, Y.H., Lu, F., Tu, Y., Ren, Z.F., 2004. Nano Lett. 4 (2), 191–195.
Liu, C., Zhang, H., Tang, Y., Luo, S., 2014. J. Mater. Chem. A 2 (13), 4580–4587.
Liu, Y., Du, Y., Li, C.M., 2013. Electroanalysis 25 (4), 815–831.
Mani, V., Devadas, B., Chen, S.M., 2013. Biosens. Bioelectron. 41, 309–315.
Mohd Omar, F., Abdul Aziz, H., Stoll, S., 2014. Sci. Total Environ. 468–469, 195–201.
Norouzi, P., Ganjali, H., Larijani, B., Ganjali, M.R., Faridbod, F., Zamani, H.A., 2011. Int. J. Electrochem. Soc. 6 (11), 5189–5199.
Oliver, N.S., Toumazou, C., Cass, A.E.G., Johnston, D.G., 2009. Diabet. Med. 26 (3), 197–210.
Periasamy, A.P., Chang, Y.J., Chen, S.M., 2011. Bioelectrochemistry 80 (2), 114–120.
Raoufi, D., 2013. Renew. Energy 50, 932–937.
Shao, Y.Y., Wang, J., Wu, H., Liu, J., Aksay, I.A., Lin, Y.H., 2010. Electroanalysis 22 (10), 1027–1036.
Sharma, P., Bhalla, V., Dravid, V., Shekhawat, G., Jinsong-Wu, Prasad, E.S., Suri, C.R., 2012. Sci. Rep. 2, 877.
Si, Y., Samulski, E.T., 2008. Nano Lett. 8 (6), 1679–1682.
Sljukic, B., Banks, C.E., Salter, C., Crossley, A., Compton, R.G., 2006. Analyst 131 (5), 670–677.
Stankovich, S., Dikin, D.A., Dommett, G.H.B., Kohlhaas, K.M., Zimney, E.J., Stach, E.A., Piner, R.D., Nguyen, S.T., Ruoff, R.S., 2006. Nature 442 (7100), 282–286.
Stoller, M.D., Park, S.J., Zhu, Y.W., An, J.H., Ruoff, R.S., 2008. Nano Lett. 8 (10), 3498–3502.
Tang, H., Chen, J., Yao, S., Nie, L., Deng, G., Kuang, Y., 2004. Anal. Biochem. 331 (1), 89–97.
Tsai, Y.-C., Li, S.-C., Chen, J.-M., 2005. Langmuir 21 (8), 3653–3658.
Umar, A., 2010. In: Umar, A., Hahn, Y.B. (Eds.), Metal Oxide Nanostructures and Their Applications, vol. 5. American Scientific Publishers, California, pp. 321–354.
Unnikrishnan, B., Palanisamy, S., Chen, S.-M., 2013. Biosens. Bioelectron. 39 (1), 70–75.
Wan, Q., Li, Q.H., Chen, Y.J., Wang, T.H., He, X.L., Li, J.P., Lin, C.L., 2004. Appl. Phys. Lett. 84 (18), 3654–3656.
Wang, J., 2008. Chem. Rev. 108 (2), 814–825.
Weber, J., Jeedigunta, S., Kumar, A., 2008. J. Nanomater. 2008, 638523.
Williams, G., Kamat, P.V., 2009. Langmuir 25 (24), 13869–13873.
Wu, X., Zhao, F., Varcoe, J.R., Thumser, A.E., Avignone-Rossa, C., Slade, R.C., 2009. Bioelectrochemistry 77 (1), 64–68.
Xiaofei, W., Ruiyi, L., Zaijun, L., 2014. RSC Adv. 4 (20), 9935–9941.
Zang, J.F., Li, C.M., Cui, X.Q., Wang, J.X., Sun, X.W., Dong, H., Sun, C.Q., 2007. Electroanalysis 19 (9), 1008–1014.
Zhou, M., Zhai, Y.M., Dong, S.J., 2009. Anal. Chem. 81 (14), 5603–5613.